OPTICS

Nonreciprocal lasing in topological cavities of arbitrary geometries

Babak Bahari, Abdoulaye Ndao, Felipe Vallini, Abdelkrim El Amili, Yeshaiahu Fainman, Boubacar Kanté*

Resonant cavities are essential building blocks governing many wave-based phenomena, but their geometry and reciprocity fundamentally limit the integration of optical devices. We report, at telecommunication wavelengths, geometry-independent and integrated nonreciprocal topological cavities that couple stimulated emission from one-way photonic edge states to a selected waveguide output with an isolation ratio in excess of 10 decibels. Nonreciprocity originates from unidirectional edge states at the boundary between photonic structures with distinct topological invariants. Our experimental demonstration of lasing from topological cavities provides the opportunity to develop complex topological circuitry of arbitrary geometries for the integrated and robust generation and transport of photons in classical and quantum regimes.

oon after the advent of quantum mechanics, Bloch established the theory of the electronic band structure of solids (electrons are fermions), resulting in the classification of materials as either electrical conductors or insulators (1). It was later understood that the band structure of fermionic systems obeys a more sophisticated classification beyond Landau's spontaneous symmetry breaking theory (2). Fermionic materials known as topological insulators are insulators in their bulk but conductors at their interfaces. Topological classifications can be extended to bosonic systems, namely photonic crystals (3, 4), which also possess a band structure obeying Bloch's theorem (5, 6). Experimental demonstration of robust electromagnetic transport in microwaves followed (7), and topological order has since been shown to be ubiquitous in many

areas of wave physics, including microwaves, acoustics, excitonics, and plasmonics (8-17). However, demonstrations in systems with broken timereversal symmetry have until now been limited to the passive topological transport of electromagnetic waves at low frequencies. Proposals to increase the operating frequency from microwaves to terahertz and the optical regime have been put forward for various platforms with and without time-reversal symmetry breaking (18-23). Topological lasing has been proposed in two dimensions using arrays of ring resonators with no time-reversal symmetry breaking (24), in one-dimensional resonant periodic crystals (25), and in a one-dimensional lattice of polariton micropillars that implements an orbital version of the Su-Schrieffer-Heeger Hamiltonian (26). However, these systems cannot implement cavities of arbitrary shapes because of their preserved time-reversal symmetry (27). An elusive implication of topology is the existence of a new class of geometry-independent photonic components. For example, the possibility of constructing geometry-independent cavities (28, 29) opens a new paradigm in cavity quantum electrodynamics and photonic integration, as it enables denser packing of components and sources of arbitrary form factors. Realizing this prospect would alleviate the constraints to use preset cavities that leave much chip space unused. Topology also naturally addresses the pressing need for nonreciprocal components that protect sources against backscattering.

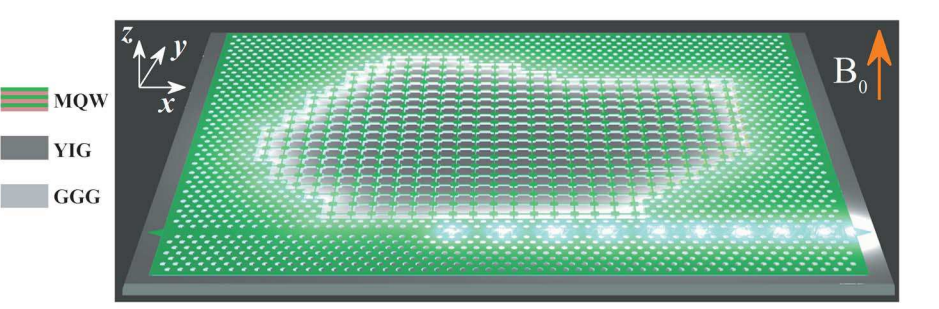
We report nonreciprocal single-mode lasing from topological cavities of arbitrary geometries operating at room temperature and at telecommunication wavelengths. The integrated nonreciprocal topological cavities, using a static magnetic field to break time-reversal symmetry, couple stimulated emission from one-way photonic edge states to a selected waveguide output with an isolation ratio in excess of 10 dB. The proposed platform has implications for integrated photonics, in which information can robustly flow between sectors characterized by different topological indices.

Our topological cavity platform (Fig. 1) is made of arbitrarily shaped closed contours that constitute the cavity and a waveguide to which the cavity is evanescently coupled. The structures are made of structured InGaAsP multiple quantum wells bonded on yttrium iron garnet (YIG), a gyrotropic material grown on gadolinium gallium garnet (GGG) by molecular beam epitaxy. The YIG substrate is used to break time-reversal symmetry in the system under a static external magnetic field (EMF). The closed contour (cavity) is defined by two different photonic crystals (PhCs). The PhC enclosed by the cavity (inside the contour) is a square lattice with a star-shaped unit cell. The PhC not enclosed by the contour constitutes the rest of the system; it is made of a triangular lattice with cylindrical air hole unit cells. A defect waveguide coupled to the cavity is created by removing a line of air holes in the PhC with the triangular lattice. Distinct topological invariants of the two PhCs will ensure the existence of robust one-way edge states at their interface, creating a one-way topological cavity that will

Department of Electrical and Computer Engineering, University of California, San Diego, La Jolla, CA 92093, USA. *Corresponding author. Email: bkante@ucsd.edu

Fig. 1. Principle of an arbitrarily shaped and integrated topological cavity. The topological cavity is an arbitrarily shaped closed contour formed between the boundaries of two photonic structures with distinct topological invariants. The structures are made of InGaAsP multiple quantum wells (MQW), bonded on yttrium iron garnet (YIG) that had been grown on gadolinium gallium garnet (GGG) by molecular beam epitaxy. The YIG substrate is used to break time-reversal symmetry in the system under a static external magnetic field (EMF). The photonic crystal (PhC) enclosed by the cavity (inside the contour) is a

square lattice with a star-shaped unit cell. The photonic crystal not enclosed by the contour constitutes the rest of the system, and, is made of a triangular lattice with cylindrical air hole unit cells. A defect waveguide is evanescently coupled to the cavity and is created by removing a line of air holes in the PhC with a triangular lattice. The topological one-way edge state circulating around the cavity is evanescently coupled to the defect waveguide, resulting in



emission at one output of the waveguide. The direction of emission can be reversed by flipping the sign of the EMF. For example, under an EMF and optical pumping from the top of the device, a counterclockwise topological edge state will preferentially couple its emission to the right output of the waveguide. Light from the tapered waveguide is then collected and analyzed using a lensed fiber connected to an optical spectrum analyzer.

couple its emission either to the right or the left output of the waveguide, depending on the direction of the EMF. For example, a counterclockwise topological edge state, as shown in Fig. 1, will preferentially couple its emission to the right output of the waveguide.

Band diagrams of the two PhCs were calculated using the finite-element method. Figure 2A shows the band diagram of the square-lattice PhC in the presence of an EMF $\mathbf{B} = B_0 \mathbf{e}_z$, where $B_0 =$ +100 Oe and \mathbf{e}_{z} is the unit vector along the direction perpendicular to the plane of the PhC. This magnetic field saturates the YIG material, maximizing the nondiagonal components of its dielectric permittivity tensor (30, 31). Initially, the EMF is zero and the band structure does not exhibit any gap in the frequency range of interest. Application of the EMF $(+B_0)$ opens a narrow band gap (green shaded region in Fig. 2A) with a width of $\Delta\lambda \sim 42$ pm. The sum of the topological invariant, also known as the Chern number (4, 7), associated with each bulk mode below the corresponding band gap is $|\Sigma C| = 1$ (31). This band gap is called nontrivial band gap because of the nonzero sum of the Chern numbers (4). Although the small nontrivial gap (restricted by the gyromagnetism strength of materials at optical frequencies) puts a limitation on some applications, it provides sufficient feedback for lasing cavities.

One-way interfaces can be implemented using another PhC with a different topological invariant (Fig. 2B). Here, the PhC with the triangular lattice possesses a broad band gap regardless of the amplitude of the EMF. The band diagram was calculated for the same EMF as the nontrivial PhC. Calculations indicate a zero sum of Chern numbers for modes below this gap that is thus called the trivial band gap (31). The dispersion of the one-way edge state at the interface between the two PhCs is shown in (31). The dimensions of the two PhCs were chosen to overlap their band gaps around the telecommunication wavelength $\lambda \sim 1.5 \mu m$, where the gain of InGaAsP material peaks. The closed contour between the trivial and nontrivial photonic structures constitutes the topological cavity that, in principle, can have arbitrary geometries while maintaining its resonant frequency. The dissimilar topology of the two band gaps is numerically verified in Fig. 2, C and D. A point source with a wavelength in the band gap of the two crystals is placed at the interface between the two PhCs. The energy of the source is confined at the interface and propagates to the right for an EMF of $+B_0e_z$ (Fig. 2C). By reversing the direction of the EMF ($-B_0\mathbf{e_z}$), propagation to the right is forbidden, demonstrating the existence of a one-way edge state.

To demonstrate the versatility of the proposed platform, we first investigated a square cavity coupled to the waveguide. The total length of the nontrivial cavity and the coupling length between the cavity and the waveguide were optimized for the edge mode (31). The structure was fabricated by electron beam lithography followed by dry etching to form the trivial and nontrivial PhCs. The PhCs were subsequently bonded on a flat YIG substrate coated with a thin layer of poly(methyl methacrylate). Finally, the InP substrate, on which InGaAsP was epitaxially grown, was removed by wet etching with hydrochloric acid (31). Figure 3A presents a top-view scanning electron micrograph (SEM) of a fabricated device where the trivial and nontrivial PhCs together with the waveguide can be seen. The fabrication is uniform over the entire area of the device.

The devices were optically pumped from the top with a pulsed laser (λ_{pump} = 1064 nm, pulse T = 12 ns at a repetition rate f = 275 kHz) using a microphotoluminescence setup. The size of the pump beam was controlled to cover the whole area of the device. Shown in Fig. 3, B and C, are real-space camera images of the surface of the devices without ($B_0 = 0$) and with ($B_0 = +100 \text{ Oe}$) EMF, respectively, for a pump power density of $\rho = 0.9 \,\mu\text{W}/\mu\text{m}^2$. An edge mode localized at the interface between the two PhCs was observed in the presence of the EMF (Fig. 3C); it disappeared when the EMF was turned off (Fig. 3B).

To further characterize the device and demonstrate the unidirectionality of the edge mode, we coupled a lensed fiber to one of the outputs of the waveguide. The outputs of the waveguides were tapered to ensure efficient coupling to the

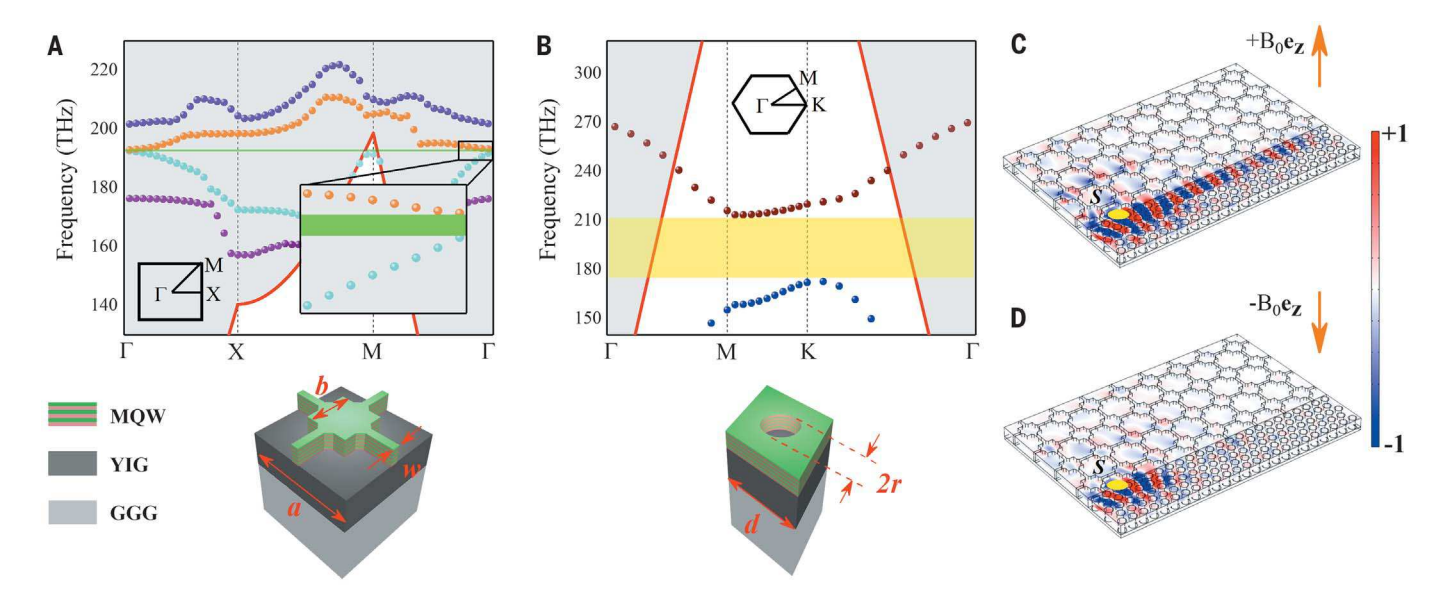
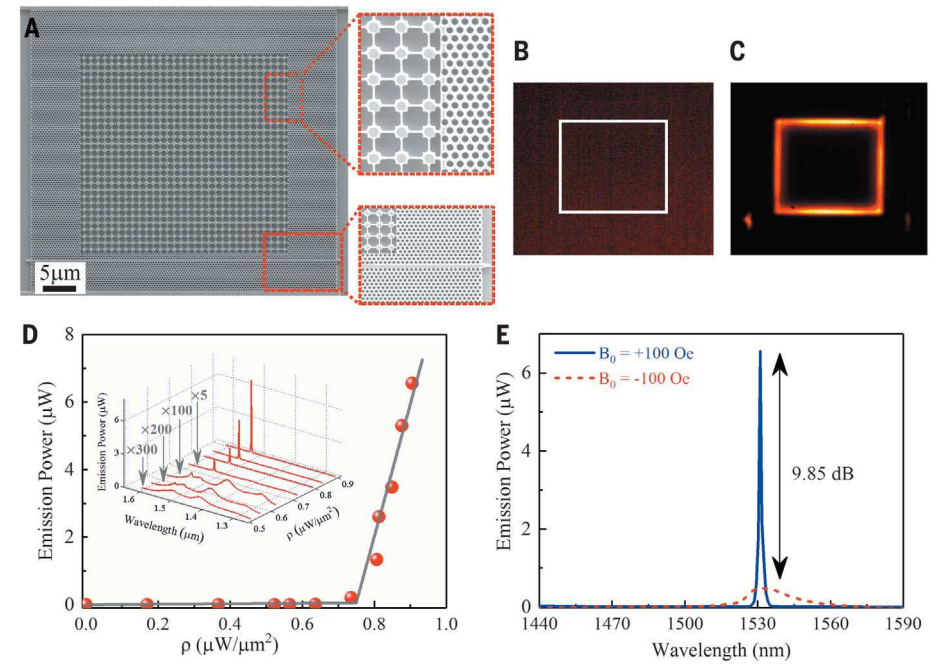


Fig. 2. Design of the nontrivial and trivial photonic structures and full-wave simulation of the edge mode. (A) Photonic band diagram of a star-shaped PhC; a unit cell is shown below. The PhC is made of InGaAsP material and has a square with dimensions a = 1084 nm (period), b =0.46a, and w = 0.0844a. The band diagram of the square-lattice PhC is calculated in the presence of an EMF that saturates the YIG material and thus maximizes the nondiagonal component of its dielectric permittivity tensor. Initially, the EMF is zero and the band structure does not exhibit any gap in the frequency range of interest (not shown). The application of the EMF $(+B_0)$ opens a narrow band gap (green shaded region) with a width $\Delta\lambda \sim 42$ pm. The sum of the topological invariant, also known as Chern number (4, 7), associated with each bulk mode below the

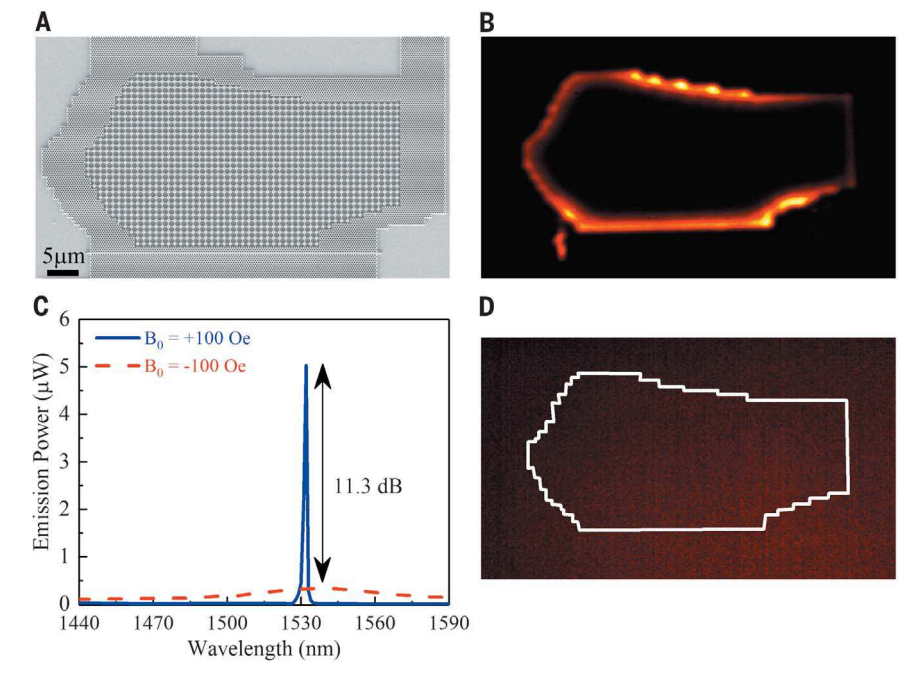
corresponding band gap is $|\Sigma C| = 1$ (31). Red solid lines represent the light cone. (B) Photonic band diagram of a triangular-lattice PhC with cylindrical air hole unit cells (shown below) in the presence of the same EMF as in (A). The periodicity d and radius of holes r are a/3 and 0.35d, respectively. A broad band gap is obtained, almost independent of the amplitude of the EMF. Calculations indicate zero for the sum of the Chern numbers of modes below this gap (31). (C and D) The boundary between these two PhCs with overlapping band gaps thus supports oneway edge states that propagate either to the right (C) or to the left (D), depending on the direction of the EMF. In the two cases, the thicknesses of the InGaAsP and YIG are 300 nm and 200 nm, respectively. Band diagrams are calculated along their respective irreducible Brillouin zones.

Fig. 3. Experimental evidence of the edge mode and unidirectional lasing from a square-shaped topological cavity. (A) Topview SEM of a fabricated square-shaped topological cavity where the trivial and nontrivial PhCs together with the waveguide can be seen. Structures were fabricated on InGaAsP by electron beam lithography followed by dry etching and then bonded on a YIG substrate with a thin layer of poly(methyl methacrylate). The InP substrate, on which InGaAsP is epitaxially grown, was subsequently removed by wet etching with hydrochloric acid (31). (B and C) Real-space camera images of the top of the device without (B) and with (C) EMF under optical pumping, using a laser with wavelength of 1064 nm. An edge mode localized at the interface between the two PhCs is unambiguously observed in the presence of the EMF; it disappears when the EMF is turned off. (D) Evolution of the output power collected by a lensed fiber coupled to the output of the waveguide as a function of pump power density and wavelength. Red dots are experimental measurements of the output power for different pump power densities when the EMF is turned on. Gray solid lines are linear



fits to the data in spontaneous and stimulated emission regimes and clearly show a threshold behavior (i.e., lasing). No lasing is observed in the absence of EMF (31). (**E**) Emission power for a pump power density of $\rho = 0.9 \,\mu\text{W}/\mu\text{m}^2$ (lasing regime) for two opposite values of the EMF ($+B_0$ and $-B_0$), which is equivalent to collecting emission from the two outputs of the waveguide with the advantage of avoiding coupling discrepancies. An isolation ratio of 9.85 dB was experimentally observed, confirming nonreciprocal lasing.

Fig. 4. Geometry-independent cavity and nonreciprocal lasing. (A) Top-view SEM of a fabricated arbitrarily shaped topological cavity with a geometry approximating a flipped USA-like map. The structure is fabricated using the same process as in Fig. 3. The shape of the cavity is deformed to investigate the geometry independence of the topological cavities; the optical length is the same as in the cavity of Fig. 3. The coupling length between the cavity and the waveguide is also unchanged. (B) Real-space camera image of the top of the device under high-power optical pumping ($\rho = 0.9 \,\mu\text{W}/\mu\text{m}^2$ at $\lambda_{\text{pump}} = 1064 \,\text{nm}$) and with the EMF turned on. An edge mode that is confined at the boundary of the topologically distinct photonic structures is clearly observed. (C) Photoluminescence spectrum of the topological cavity for two opposite values of the EMF for a pump power density of $\rho = 0.9 \,\mu\text{W/}\mu\text{m}^2$ (lasing regime). As shown, for a forward bias $(+B_0)$, the cavity lases with stimulated emission, but for a backward bias $(-B_0)$, a strong suppression of emission is obtained with an isolation ratio between ports of 11.3 dB. (D) The edge mode disappears when the EMF is turned off because the nontrivial band gap closes.



fiber. The coupling was aided by a piezoelectric positioning device with nanometer resolution. The tip of the lensed fiber was placed in front of the waveguide, and the other end of the fiber was directly connected to an optical spectrum analyzer.

Figure 3D shows the evolution of the output power as a function of both pump power den-

sity and wavelength. By varying the pump power density with the EMF turned on, a threshold behavior with a clear transition from spontaneous emission to stimulated emission (lasing) was observed. Turning off the EMF resulted in the suppression of lasing (31).

To prove that lasing is from a one-way edge mode, we flipped the direction of the EMF by reversing the current in the solenoid creating $\mathbf{B} = -B_0\mathbf{e}_z$ and measured the emitted power and its spectrum. This is equivalent to coupling the fiber to the other end of the waveguide for a fixed direction of the EMF, with the advantage of avoiding discrepancies between the coupling efficiencies to the two ends of the waveguide, thus enabling quantitative comparison of the emissions.

Figure 3E presents the output emission power of the structure for two opposite values of the EMF ($+B_0$ and $-B_0$) for the same pump power density ($\rho = 0.9 \,\mu\text{W}/\mu\text{m}^2$) in the lasing regime. As seen, there is a large reduction in the luminescence spectrum; we measured an isolation ratio of 9.85 dB. In nontopological cavities with broken time-reversal symmetry (that cannot have arbitrary shapes), the clockwise (CW) and counterclockwise (CCW) modes of the cavity have similar characteristics but a small wavelength shift (30). However, in topological cavities, one of the modes, either the CW or the CCW, is forbidden, depending on the direction of EMF, and thus cannot be excited, ensuring single-mode operation. This is a fundamental difference between these systems, as nontopological cavities will exhibit two slightly detuned modes that both lie within the broad-gain bandwidth of the semiconductor and would thus give rise to mode competition.

Topological edge modes are robust against backscattering from imperfections and sharp corners. Beyond robust and passive transport, this implies the possibility of implementing deformed cavities of arbitrary geometries. Figure 4A shows a top-view SEM of an arbitrarily shaped cavity with a geometry approximating a flipped USAlike map with the same optical length as the square cavity. We optically pumped the device from the top, then collected and analyzed the emission from the tapered waveguide, again using the lensed fiber. When the EMF was turned on, realspace imaging of the top of the device (Fig. 4B) provided evidence for an edge mode that is tightly confined at the boundary of the topologically distinct photonic structures. When the EMF was turned off, the edge mode disappeared (Fig. 4D). Unidirectional lasing with an isolation ratio of 11.3 dB was experimentally achieved with a pump power density $\rho = 0.9 \,\mu\text{W/}\mu\text{m}^2$ (Fig. 4C). See (31) for additional deformed cavities of different shapes.

We experimentally demonstrated nonreciprocal lasing from topological cavities of arbitrary geometries. By evanescently coupling the topological cavities to waveguides, stimulated emission from one-way modes is coupled to a selected waveguide output with an isolation ratio as large as 11.3 dB. These results demonstrate the flexibility of topological cavities and open avenues in photonic integration where information can robustly flow between sectors characterized by their topological invariants. This work will enable the investigation of nontrivial photonic devices.

REFERENCES AND NOTES

- 1. N. W. Ashcroft, N. D. Mermin, Solid State Physics (Holt, Rinehart and Winston, 1976).
- 2. M. Z. Hasan, C. L. Kane, Rev. Mod. Phys. 82, 3045–3067 (2010).
- 3. F. D. M. Haldane, S. Raghu, Phys. Rev. Lett. 100, 013904 (2008).
- 4. S. Raghu, F. D. M. Haldane, Phys. Rev. A 78, 033834 (2008). E. Yablonovitch, Phys. Rev. Lett. 58, 2059-2062 (1987).
- 6. S. John, Phys. Rev. Lett. 58, 2486-2489 (1987).
- Z. Wang, Y. Chong, J. D. Joannopoulos, M. Soljacić, Nature 461, 772-775 (2009)
- Y. Poo, R. X. Wu, Z. Lin, Y. Yang, C. T. Chan, Phys. Rev. Lett. 106, 093903 (2011).
- 9. M. C. Rechtsman et al., Nat. Photonics 7, 153-158 (2012).
- 10. A. B. Khanikaev et al., Nat. Mater. 12, 233-239 (2013).
- 11. Y.-J. Chen et al., Nat. Commun. 5, 5782 (2014).
- 12. X. Cheng et al., Nat. Mater. 15, 542-548 (2016).
- 13. A. P. Slobozhanyuk et al., Sci. Rep. 6, 22270 (2016).
- 14. A. B. Khanikaev, R. Fleury, S. H. Mousavi, A. Alù, Nat. Commun. 8260 (2015).
- 15. R. Fleury, A. B. Khanikaev, A. Alù, Nat. Commun. 7, 11744 (2016).
- 16. J. Yuen-Zhou, S. K. Saikin, N. Y. Yao, A. Aspuru-Guzik, Nat. Mater. 13, 1026-1032 (2014).
- 17. D. Jin et al., Phys. Rev. Lett. 118, 245301 (2017).
- 18. B. Bahari, R. Tellez-Limon, B. Kanté, Appl. Phys. Lett. 109, 143501 (2016).
- 19. M. C. Rechtsman et al., Nature 496, 196-200 (2013).
- 20. M. Hafezi, S. Mittal, J. Fan, A. Migdall, J. M. Taylor, Nat. Photonics 7, 1001-1005 (2013).
- 21. Y. Plotnik et al., Nat. Mater. 13, 57-62 (2014).

- 22. A. P. Slobozhanyuk, A. N. Poddubny, A. E. Miroshnichenko, P. A. Belov, Y. S. Kivshar, Phys. Rev. Lett. 114, 123901 (2015).
- 23. A. Slobozhanyuk et al., Nat. Photonics 11, 130-136 (2016).
- 24. S. Wittek, G. Harari, M. A. Bandres, H. Hodaei, M. Parto,
- P. Aleahmad, M. C. Rechtsman, Y. D. Chong, D. N. Christodoulides, M. Khajavikhan, M. Segev,
- in Conference on Lasers and Flectro-Optics, OSA Technical Digest (Optical Society of America, 2017), paper FTh1D.3.
- 25. L. Pilozzi, C. Conti, Phys. Rev. B 93, 195317 (2016).
- 26. P. St-Jean et al., Lasing in topological edge states of a 1D lattice, arXiv:1704.07310 (2017).
- 27. J. Noh, S. Huang, K. Chen, M. C. Rechtsman, Observation of photonic topological valley-Hall edge state. arXiv:1706.00059 (2017).
- 28. I. Liberal, A. M. Mahmoud, N. Engheta, Nat. Commun. 7, 10989
- 29. T. Ma. G. Shvets. New J. Phys. 18, 025012 (2016).
- 30. L. Bi et al., Nat. Photonics 5, 758-762 (2011).
- 31. See supplementary materials.

ACKNOWLEDGMENTS

Supported by Office of Naval Research Young Investigator Award N00014-17-1-2671; NSF Career Award ECCS-1554021; U.S. Department of Energy grant EE0007341; NSF grants ECCS-1405234, ECCS-1507146, and CCF-1640227; Office of Naval Research Multi-University Research Initiative grant N00014-13-1-0678; Army Research Office grant W911NF-16-1-0245; the Semiconductor Research Corporation; and startup funds provided to B.K. by the University of California, San Diego. The work was performed in part at the San Diego Nanotechnology Infrastructure, a member of the National Nanotechnology Coordinated Infrastructure, which is supported by NSF grant ECCS-1542148. We thank M. I. Montero Ramirez for technical assistance regarding electron beam lithography and T. Lepetit for helpful discussions. The Regents of the University of California have filed a patent on systems and applications using devices based on topological cavities.

SUPPLEMENTARY MATERIALS

www.sciencemag.org/content/358/6363/636/suppl/DC1 Supplementary Text Figs. S1 to S11 Reference (32)

22 July 2017; accepted 28 September 2017 Published online 12 October 2017 10.1126/science.aao4551



Nonreciprocal lasing in topological cavities of arbitrary geometries

Babak Bahari, Abdoulaye Ndao, Felipe Vallini, Abdelkrim El Amili, Yeshaiahu Fainman and Boubacar Kanté

Science 358 (6363), 636-640.

DOI: 10.1126/science.aao4551originally published online October 12, 2017

Topological lasing

Resonant cavities that confine light are crucial components of lasers. Typically, these cavities are designed to high specification to get the best possible output. That, however, can limit their integration into photonic devices and optical circuits. Bahari et al. fabricated resonant cavities of arbitrary shape within a hybrid photonic crystal structure. The confinement of light to topologically protected edge states resulted in lasing at communication wavelengths. Relaxing the resonant cavity design criteria should be useful in designing photonic devices. Science, this issue p. 636

ARTICLE TOOLS http://science.sciencemag.org/content/358/6363/636

SUPPLEMENTARY MATERIALS http://science.sciencemag.org/content/suppl/2017/10/11/science.aao4551.DC1

REFERENCES This article cites 26 articles, 0 of which you can access for free

http://science.sciencemag.org/content/358/6363/636#BIBL

PERMISSIONS http://www.sciencemag.org/help/reprints-and-permissions

Use of this article is subject to the Terms of Service